Dalton Transactions

Cite this: *Dalton Trans.*, 2011, **40**, 6524

www.rsc.org/dalton

PAPER

New ammonium surfactant-stabilized rhodium(0) colloidal suspensions: Influence of novel counter-anions on physico-chemical and catalytic properties

Elodie Guyonnet Bilé,[a,b] Rita Sassine,[c] Audrey Denicourt-Nowicki,[a,b] Franck Launay[c] and Alain Roucoux*[a,b]

Received 14th December 2010, Accepted 7th April 2011
DOI: 10.1039/c0dt01763a

Novel anionic species, such as hydrogen carbonate (HCO_3^-), fluoride (F^-), triflate ($CF_3SO_3^-$), tetrafluoroborate (BF_4^-) and chloride (Cl^-) were investigated as new partners of water soluble *N*,*N*-dimethyl-*N*-cetyl-*N*-(2-hydroxyethyl) ammonium salts, used as a protective agent of rhodium colloids. The effect of the surfactant polar head on the micellar behavior, size and morphology of the nanospecies was studied by adapted physico-chemical experiments (surface tension measurements, dynamic light scattering, thermogravimetric and TEM analyses) and discussed in terms of strong or weak stabilization of the growing nanoparticles surface. Finally, the influence of the nanoenvironment generated by the surfactant with various counter-anions was evaluated *via* the hydrogenation of aromatics.

1 Introduction

In recent years, economic and ecological priorities have pressed the scientific community to promote clean processes and technologies. For that reason, the development of catalysis in water has emerged as an environmental friendly approach[1] and noble metal nanocatalysts in particular have proved their effectiveness.[2] Among the various protective agents applied to efficiently stabilise colloids in water, such as cyclodextrins,[3–11] water soluble polymers,[12–15] phosphine[16–18] or citrate[19,20] derivatives, several lipophilic ammonium salts bearing a long alkyl chain, such as cetyldimethylammonium bromide (CTABr) and its derivatives, have been widely used and studied in the synthesis of Pd, Rh or Ru nanoparticles (NPs).[21–23] These surfactants avoid undesired agglomeration due to a combination of steric and electrostatic interactions called electrosteric protection at the particle surface, according to the Derjaguin–Landau–Verway–Overbeek (DLVO) theory used to rationalize this stabilisation effect.[24–25] In fact, the thermodynamically unstable metallic nanoparticles are protected by a double layer of amphiphilic molecules around the metal core, as previously demonstrated by Chen[26–27] and El Sayed[28] for Cu and Ni NPs or Au nanorods. The modulation of the positive charge on the metal surface is clearly a consequence of the anion adsorption and, in many cases, the presence of a halogen, such as chloride, or other anions near the electron deficient nanoparticle surface was demonstrated.[29–30] Various zero-valent nanoparticles (1–10 nm in size), obtained by reduction of metallic precursors, have been prepared in the presence of tetraalkylammonium salts, which have proved to be interesting as they play dual roles of the protective agent and the mass-transfer promoter. The obtained nanocatalysts were used in various reactions, including hydrogenation, C–C coupling and oxidation and they have been widely described in recent reviews[22–23,31–32] and book chapters.[33]

Our approach is to use colloidal metallic particles finely dispersed in water and to investigate their catalytic properties in pure biphasic water–liquid systems without any organic solvent.[34–37] To facilitate the recycling process, the colloids must be stabilized by highly water-soluble protective agents. During the last few years, we have developed the facile synthesis of *N*,*N*-dimethyl-*N*-alkyl-*N*-(2-hydroxyethyl) ammonium salts (HEA salts) with various alkyl chain lengths (up to 18 carbon atoms) and optimized their application to maintain the catalytic species within the aqueous phase.[35,38] In this paper, we describe the synthesis of a series of original surfactants HEA16X bearing a lipophilic chain with 16 carbon atoms, modulated by the nature of the counter-anion X. In particular, we prepared a new series of ammonium salts with anions, such as hydrogen carbonate (HCO_3^-), fluoride (F^-), tetrafluoroborate (BF_4^-) and triflate ($CF_3SO_3^-$), and compared them to the previously described HEA16Cl. These new compounds and their ability to provide stable aqueous suspensions were investigated and fully characterized by various techniques, including surface tension measurements, dynamic light scattering (DLS), thermogravimetric analysis (TGA) and TEM experiments. Finally, the effect of the counter-anion of the ammonium salt was evaluated in catalysis under micellar conditions. According to the effect of the counter-anion in partnership with the ammonium head group, we demonstrated that surfactant-protected colloids could be used to efficiently catalyze the hydrogenation of model aromatic compounds in pure

[a]*Ecole Nationale Supérieure de Chimie de Rennes, CNRS, UMR 6226, Avenue du Général Leclerc, CS 50837, 35708, Rennes Cedex 7. E-mail: alain.roucoux@ensc-rennes.fr*
[b]*Université Européenne de Bretagne,*
[c]*UPMC Paris 06, Laboratoire de Réactivité de Surface (LRS), CNRS, UMR 7197, site Le Raphaël, 3 Rue Galilée, 94200, Ivry-sur-Seine*

biphasic conditions (water/substrate). The stability and durability of the catalytic systems were checked through the recycling of the aqueous phase.

2 Experimental Section

2.1 Materials

Rhodium chloride hydrate was obtained from Strem Chemicals. Sodium borohydride, various functionalized cetylalkanes, *N*,*N*-dimethylethanolamine and all of the aromatic substrates were purchased from Acros or Fluka and were used without further purification. Water was distilled twice by the conventional method before use.

2.2 Analytical procedures

Transmission electron microscopy (TEM) images were recorded with a JEOL TEM 100CXII electron microscope operated at an acceleration voltage of 100 kV. The samples were prepared by the addition of a drop of the stabilized colloid in water on a copper grid coated with a porous carbon film. Any excess of the colloidal dispersion was removed after 1 min using cellulose before transfer to the microscope. Thermogravimetric analysis (TGA) data were obtained in an aluminium pan using a TA Instruments – Waters LLC SDT Q600 analyzer. The TGA data were collected at 10 °C min^{-1} under air flow (100 mL min^{-1}). To determine the CMC (critical micellar concentration) and the nature of the interaction between the molecules, the surface tension was determined as a function of the concentration. The measurements were performed using an automatic tensiometer (Krüss K100) and the DuNoüy Ring Method for air–water interfaces at 296 K. Before each experiment, the platinum ring was cleaned in a water/ethanol mixture and then in a blue flame. A concentrated solution (6 mL) was introduced to a conical vessel (165.7 mL) and this was diluted by the addition of small amounts of ultrapure water. After each addition, the solution was stirred for 120s. The immersion depth of the ring was 1 mm. The equilibrium surface tension was measured three times at 23 °C for each concentration using the Harkins and Jordan correction method. The hydrodynamic size D_h and zeta potential ζ of the nanoparticle aggregates were measured by dynamic light scattering (DLS) using a DelsaNano C instrument (Beckmann Coulter). The aqueous suspensions of rhodium nanoparticles were analysed at 25 °C and measurements were started 10 min after the cell was placed in the DLS apparatus to allow the temperature to equilibrate.

2.3 Synthesis of surfactants HEA16X

The compounds were prepared as previously described or after modification and were fully characterized.[39–41] ^{1}H, ^{13}C and ^{19}F NMR spectra were recorded on a BRUKER Avance III 400 spectrometer at 400.13 MHz for ^{1}H, 100.61 MHz for ^{13}C and 376.50 MHz for ^{19}F. Chemical shifts ($CDCl_3$ or D_2O) are given as δ (ppm), measured downfield from tetramethylsilane (TMS) and $CFCl_3$ as external references.

2.3.1 Synthesis of *N*,*N*-dimethyl-*N*-cetyl-*N*-(2-hydroxyethyl) ammonium chloride HEA16Cl. Chlorohexadecane (1.2 eq.) and *N*,*N*-dimethylethanolamine (1 eq.) were refluxed in absolute ethanol for 48 h. Then, the solvent was removed under reduced pressure. The obtained solid was washed twice with diethyl ether to afford a white solid with a good yield (92%), m.p. 204 °C. ^{1}H NMR ($CDCl_3$): δ = 0.81 (t, J = 7.1 Hz, 3H), 1.18 (m, 24H), 1.27 (m, 2H), 1.67 (m, 2H), 3.30 (s, 6H), 3.48 (m, 2H), 3.65 (m, 2H), 4.03 (m, 2H), 4.61 (m, 1H). ^{13}C NMR ($CDCl_3$): δ = 14.09, 22.7–31.9, 52.0, 55.9, 65.7, 66.0 ppm. ^{1}H NMR (D_2O): δ = 0.80 (t, J = 6.8 Hz, 3H), 1.21–1.28 (m, 27H), 1.70 (m, 2H), 3.09 (s, 6H), 3.34 (m, 2H), 3.44 (m, 2H), 3.94 (m, 2H) ppm. ^{13}C NMR (D_2O): δ = 13.87, 22.45–32.03, 51.55, 55.41, 65.04, 65.7, 66 ppm. Elemental analysis: Calcd (%) for $C_{20}H_{44}ClNO$ (350 g mol^{-1}): C 68.63, H 12.67; found: C 68.59, H 12.69.

2.3.2 General procedure for the preparation of *N*,*N*-dimethyl-*N*-cetyl-*N*-(2-hydroxyethyl) ammonium X salts with X = HCO_3^-, F^-, BF_4^-, $CF_3SO_3^-$. The surfactants HEA16X were prepared by ion exchange reactions in acetone or methanol with HEA16Cl and the appropriate alkaline ($NaHCO_3$, $NaBF_4$, KF) or silver ($AgCF_3SO_3$) salt in a molar ratio of 1 : 1 under refluxing conditions. After reaction, the resulting mixture was filtered through celite and the solvent was removed to afford a white solid that did not need further purification before use for rhodium suspension synthesis.

2.3.2.1 N,N-dimethyl-N-cetyl-N-(2-hydroxyethyl)ammonium hydrogen carbonate HEA16HCO$_3$. yield: 60%. m.p. 210–215 °C. ^{1}H NMR ($CDCl_3$): δ = 0.81 (t, J = 7.1 Hz, 3H), 1.18 (m, 24H), 1.27 (m, 2H), 1.67 (m, 2H), 3.30 (s, 6H), 3.48 (m, 2H), 3.65 (m, 2H), 4.03 (m, 2H), 4.61 (m, 1H). ^{13}C NMR ($CDCl_3$): δ = 14.09, 22.7–31.9, 52.0, 55.9, 65.7, 66.0. ^{1}H NMR (D_2O): δ = 0.79 (t, J = 7.1 Hz, 3H), 1.21 (m, 27H), 1.69 (m, 2H), 3.08 (s, 6H), 3.31 (m, 2H), 3.42 (m, 2H), 3.93 (m, 2H) ppm. ^{13}C NMR (D_2O): δ = 13.84, 22.45, 26.24–32.04, 51.54, 55.38, 64.97, 65.10 ppm. Elemental analysis: Calcd (%) for $C_{21}H_{45}NO_4$ (375 g mol^{-1}): C 68.16, H 12,08; found: C 68.85, H 12.79.

2.3.2.2 N,N-Dimethyl-N-cetyl-N-(2-hydroxyethyl) ammonium fluoride HEA16F. yield: 97%. m.p. 75–80 °C. ^{1}H NMR ($CDCl_3$): δ = 0.81 (t, J = 7.1 Hz, 3H), 1.18 (m, 24H), 1.27 (m, 2H), 1.67 (m, 2H), 3.30 (s, 6H), 3.48 (m, 2H), 3.65 (m, 2H), 4.03 (m, 2H), 4.61 (m, 1H). ^{13}C NMR ($CDCl_3$): δ = 14.09, 22.7–31.9, 52.0, 55.9, 65.7, 66.0. ^{19}F NMR ($CDCl_3$): δ = –146.53. ^{1}H NMR (D_2O): δ = 0.72 (t, J = 6.8 Hz, 3H), 1.15–1.21 (m, 27H), 1.62 (m, 2H), 3.0 (s, 6H), 3.20 (m, 2H), 3.34 (m, 2H), 3.86 (m, 2H) ppm. ^{13}C NMR (D_2O): δ = 13.85, 22.35–31.97, 51.48, 55.35, 65.06 ppm. ^{19}F NMR (D_2O): δ = –122.23 ppm. Elemental analysis: Calcd (%) for $C_{20}H_{44}FNO$ (333.5 g mol^{-1}): C 71.9, H 13.19; found: C 71.19, H 12.9.

2.3.2.3 N,N-Dimethyl-N-cetyl-N-(2-hydroxyethyl) ammonium tetrafluoroborate HEA16BF$_4$. yield: 94%. m.p. 114 °C. ^{1}H NMR ($CDCl_3$): δ = 0.81 (t, J = 7.1 Hz, 3H), 1.18 (m, 24H), 1.27 (m, 2H), 1.67 (m, 2H), 3.30 (s, 6H), 3.48 (m, 2H), 3.65 (m, 2H), 4.03 (m, 2H), 4.61 (m, 1H). ^{13}C NMR ($CDCl_3$): δ = 14.09, 22.7–31.9, 52.0, 55.9, 65.7, 66.0. ^{19}F NMR ($CDCl_3$): –150.22, –150.27. ^{1}H NMR (D_2O): δ = 0.79 (t, J = 7.1 Hz, 3H), 1.21–1.26 (m, 27H), 1.66 (m, 2H), 3.04 (s, 6H), 3.26 (m, 2H), 3.39 (m, 2H), 3.93 (m, 2H). ^{13}C NMR (2D-HSQC, D_2O, 50 °C): δ = 12.5, 24–29, 51, 55, 61, 63, 66 ppm. ^{19}F NMR (D_2O): δ = –149.17; –149.22 ppm. Elemental analysis: Calcd (%) for $C_{20}H_{44}BF_4NO$ (401 g mol^{-1}): C 59.85, H 11.05; found: C 60.42, H 11.03.

2.3.2.4 N,N-Dimethyl-N-cetyl-N-(2-hydroxyethyl) ammonium triflate HEA16CF$_3$SO$_3$. yield: 90%. m.p. 95–100 °C. ^{1}H NMR ($CDCl_3$): δ = 0.81 (t, J = 7.1 Hz, 3H), 1.18 (m, 24H), 1.27 (m, 2H), 1.67 (m, 2H), 3.30 (s, 6H), 3.48 (m, 2H), 3.65 (m, 2H), 4.03 (m, 2H), 4.61 (m, 1H). ^{13}C NMR ($CDCl_3$): δ = 14.09, 22.7–31.9, 52.0, 55.9, 65.7, 66.0. ^{19}F NMR ($CDCl_3$): δ = –78.53. ^{1}H NMR (D_2O): δ = 1.08 (t, J = 7.1 Hz, 3H), 1.49–1.53 (m, 27H), 1.92 (m, 2H), 3.31 (s, 6H), 3.51 (m, 2H), 3.66 (m, 2H), 4.21 (m, 2H) ppm. ^{13}C NMR (2D-HSQC, D_2O, 50 °C): δ = 14.0, 23.0, 26.0–32.0, 52.0, 56.0, 66.0 ppm. ^{19}F NMR (D_2O): δ = –78.87 ppm. Elemental analysis: Calcd (%) for $C_{21}H_{44}F_3NO_4S$ (463 g mol^{-1}): C 54.43, H 9.5; found: C 54.53, H 9.96.

2.4 Synthesis of the aqueous rhodium(0) suspension

The suspensions were prepared at ambient temperature (20 °C). To an aqueous solution of the appropriate surfactant (95 mL, 7.6 × 10^{-3} mol L^{-1}) was added sodium borohydride (3 mg, 9.5 × 10^{-4} mol). Then, this solution was quickly added to an aqueous solution (5 mL) of the precursor $RhCl_3$ under vigorous stirring. 3 eq. of H_2O (100 mg, 3.8 × 10^{-4} mol) was added to obtain an aqueous Rh(0) colloidal suspension (100 mL). The reduction occurred instantaneously and was characterized by a color change from red to black. Measurement of the number of particles was made with an automatic counting program (Image J) using Microsoft Excel to generate histograms of the size distribution. The obtained suspensions were stable for months, as confirmed by TEM.

2.5 General procedure for hydrogenation and recycling under atmospheric hydrogen pressure

A 25 mL round bottom flask, charged with 10 mL of aqueous colloidal Rh(0) suspension and aromatic substrate ([substrate]/[metal] = 100), was connected to a gas burette (500 mL) and a flask to balance the pressure. Then, the system was filled with hydrogen and the mixture was magnetically stirred at 1500 rpm. The reaction was monitored by gas chromatography analysis. Based on the amount of introduced rhodium, the turnover frequency (TOF) was determined for 100% conversion.

2.6 General procedure for hydrogenation under hydrogen pressure

The stainless steel autoclave was charged with the previously prepared aqueous suspension of Rh(0) (10 mL) and a magnetic stirrer. The appropriate substrate (3.8 × 10^{-3} mol, 100 eq.) was added to the autoclave and dihydrogen was admitted to the system at a constant pressure (20 bar). The mixture was stirred with a magnetic stirrer. Samples were removed regularly for gas chromatography analysis. The turnover frequency was determined for 100% conversion.

3. Results and Discussion

Recently, we demonstrated that aqueous dispersions of rhodium(0) colloids are efficient nanocatalysts in hydrogenation reactions in biphasic liquid–liquid media, where the substrate and final product constitute the organic phase. We have largely studied chloride and bromide ammonium surfactants as protective agents for several metallic species (Ir, Ru, Rh, Pd) in various reactions, such as hydrogenation,[34,36,38] tandem dehalogenation–hydrogenation[42] and C–C coupling.[43] In this paper, we describe our investigations on a new series of *N*,*N*-dimethyl-*N*-cetyl-*N*-(2-hydroxyethyl) ammonium salts possessing original counter-anions (HEA16X, X = HCO_3, F, CF_3SO_3, BF_4). To the best of our knowledge, X^- species, such as hydrogen carbonate (HCO_3^-), fluoride (F^-) and triflate ($CF_3SO_3^-$), have rarely been described as counter-anions of ammonium salts or used to stabilize nanocatalysts in micellar media.

These compounds were easily synthesized by a one-step ion exchange reaction (Scheme 1) starting from the previously reported *N*,*N*-dimethyl-*N*-cetyl-*N*-(2-hydroxyethyl) ammonium chloride salt obtained by quaternisation of *N*,*N*-dimethylethanolamine with cetylchloride in EtOH.

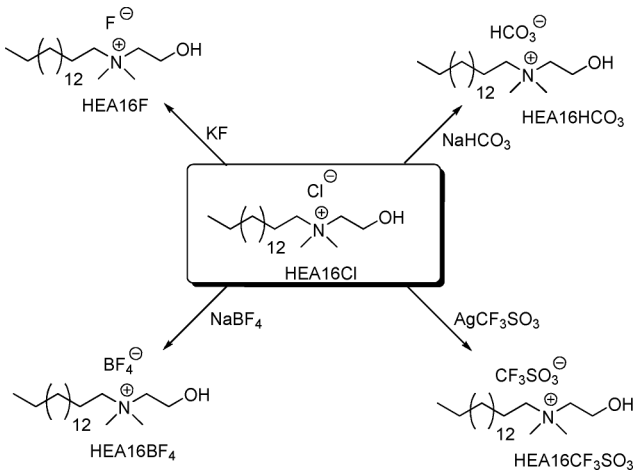

Scheme 1 The synthesis of various *N*,*N*-dimethyl-*N*-cetyl-*N*-(2-hydroxyethyl) ammonium salts (HEA16X, X = HCO_3, F, CF_3SO_3, BF_4) starting from the chloride salt.

In order to better understand the phenomena occurring at the interface during the catalytic reaction, this new family of surfactants was characterized by surface tension measurements (Table 1). Analyses were performed when equilibrium was achieved, *i.e.*, when the surface tension was constant. They demonstrated that all of the HEA16X bearing a lipophilic alkyl chain with 16 carbon atoms self-aggregate into micelles above critical micellar concentrations (CMC) of 2.12, 0.62, 0.6, 0.25 mmol L^{-1} for HEA16F, HEA16BF_4, HEA16HCO_3 and HEA16CF_3SO_3, respectively. These values were quite similar to the CMC of HEA16Cl (1.2 × 10^{-3} mol L^{-1}), which was used as a reference[39] (Table 1). The CMC values decrease in the following order: F > Cl > BF_4 ≈ HCO_3 > CF_3SO_3. Clearly, contrary to halogens, larger anions, which are more polarizable, contribute to decrease the electrostatic repulsions between the polar groups and consequently promote micelle formation. The decrease in the surface tension of the aqueous solutions of these compounds below the CMC (from 72 mN m^{-1} for pure water to about 30 mN m^{-1}) is related to their adsorption at the water/air interface, according to the Gibbs equation.

The triflate HEA16CF_3SO_3 and tetrafluoroborate HEA16BF_4 derivatives exhibit excellent surfactant properties, with a surface tension at the CMC, γ_{CMC}, of around 31 mN m^{-1}. The anions, such as fluoride, chloride and HCO_3, lead to similar reduction of the surface tension, with values of the surface tension at the

Table 1 Physico-chemical properties of HEA derivatives and their predicted aggregate geometry based on *A*

Entry	X	CMC[a] (mmol L^{-1})	γ_{CMC}[b] (mN m^{-1})	*A*[c] ($Å^2$)	CPP[d]	Geometry
1	CF_3SO_3	0.25	32.0	49.6	0.42	rods
2	BF_4	0.62[e]	30.3	37.3	0.55	rods
3	HCO_3	0.6	40.3	46.6	0.45	rods
4	F	2.12	43.2	87.1	0.24	spheres
5	Cl	1.23	40.5	33.4	0.63	bilayers

[a] CMC = critical micellar concentration, [b] γCMC = surface tension at CMC, [c] *A* = area of polar head per molecule, [d] CPP = critical packing parameter, spherical micelles for CPP <1/3, cylindrical or rod-like micelles for 1/3 < CPP < 1/2 and bilayers with CPP > 1/2. [e] CMC measured at 30 °C.

CMC of about 40 mN m^{-1}. The molecular area *A*, which is defined as the area occupied by the surfactant molecules at the air–water interface at equilibrium, was directly determined by the apparatus. HEA16X salts demonstrate significant surface areas *A*, in the range 33–87 $Å^2$. For comparison, Asai *et al.* reported an area per molecule of 62 $Å^2$ for cetyltrimethylammonium chloride, which is higher than that obtained for HEA16Cl (33 $Å^2$), showing the influence of the 2-hydroxyethyl part.[44] No correlation could be proposed regarding the nature and the size of the counter-anion. However, several parameters, such as the hydration of the hydrophilic moiety and the geometry of the head group, have already been proved to have a significant influence in determining the ease of packing of the head groups. Surfactants whose geometries allow closer packing at the interface will generally exhibit smaller surface areas.[45–46] In the halogenated series, the observed differences between HEA16F and HEA16Cl could be explained by the value of polarizability, which drives chloride towards the surface, while fluoride, as a hard ion, is repelled from the solution/vapor interface, according to molecular dynamics simulations.[47] Accordingly, the calculated critical packing parameters CPP[45–46,48] allow to predict, from simple geometric considerations, that these molecules are likely to pack as spherical micelles for HEA16F due to a CPP < 1/3 and tend to flexible bilayers for HEA16Cl with a CPP = 0.66. Finally, cylindrical micelles (rods) were proposed for HEA16X (X = BF_4, HCO_3, CF_3SO_3) with 1/3 < CPP < 1/2 (Table 1). To conclude, the newly synthesized amphiphilic compounds present surfactant behavior and mainly form rods or spherical micelles in water.

According to our previous studies,[34–35] colloidal suspensions were prepared in water at room temperature by chemical reduction of rhodium trichloride with sodium borohydride in a dilute aqueous solution of HEA16X. First, we checked the formation of a bilayer structure of the HEA16Cl salts at the particle surface to avoid agglomeration in water. The thermogravimetric curve obtained from lyophilized materials (Fig. 1) showed two weight losses, as already observed by Chen[26] in the case of CTAB molecules. The first weight loss step occurred gradually, from 200–350 °C, and the second one sharply, within 400–450 °C.

These results suggest that the inner layer is bound to the NPs' surface *via* the charged groups and that it is connected to the outer layer, whose polar groups are directed towards the aqueous solution through hydrophobic interactions. Based on these results, we could assume the formation of a bilayer of surfactants around the rhodium colloids. Nevertheless, we could not discard the potential formation in water of free micelles or surfactant aggregates as hemimicelles after the CMC,

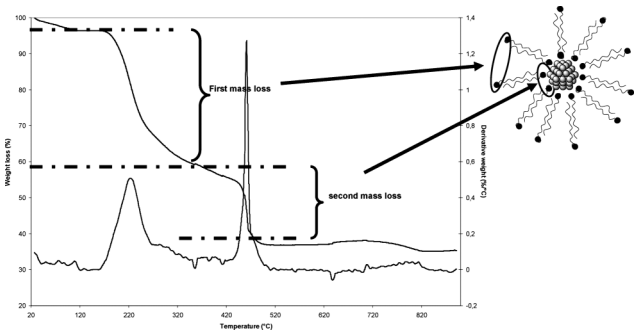

Fig. 1 The TGA curve for the HEA16Cl capped Rh(0) nanoparticles and a representation of the bilayer structure on the particle surface.

which could also help to solubilize organic substrates during the catalysis.

The particle sizes and morphologies of the Rh@HEA16X systems were determined by transmission electron microscopy. Micrographs and the size distribution are shown in Figs 2–5. The rhodium particles possess different morphologies depending on the nature of the protective agent: spherical geometries for those prepared with $HEA16HCO_3$ or the previously reported[34] HEA16Cl, and worm-like structures for HEA16X with X = BF_4 and CF_3SO_3. TEM images taken from different enlargements on a copper grid of Rh@HEA16F show a bimodal morphology with isolated and elongated (worm-like) nanoparticles (Fig. 2a). In this case, the presence of a fluoride anion promotes weaker stabilization of the spherical NPs by the surfactant, which finally induces a sintering of the nanospecies. A similar behavior could be proposed with surfactants containing fluorinated counter-anions, such as BF_4 or CF_3SO_3, which provide weaker protection at the particle surface, thus leading to their growth or sintering into worm-like nanoparticles or shorter dendrites (Figs 3b and 4). A different approach could also be considered according to the work reported by Shelnutt on the synthesis of a platinum nanowire network in the presence of a soft template formed by CTABr for particle growth in a two-phase water–chloroform system. In that case, the formation of worm-like NPs was attributed to the supramolecular organization of the surfactant into worm-like micelles.[49] Nevertheless, this explanation was not suitable considering the use of pure water media.

The significant role of the weakly coordinating BF_4 in the formation of worm-like structures for Ir(0) colloids was demonstrated by Finke[50,51] in high dielectric constant solvents (ε = 69 and 165 for propylene carbonate and *N*-methylacetamide, respectively, compared with ε = 80 for H_2O). The putative influence of the coordination of the ligand as a factor providing worm-like and

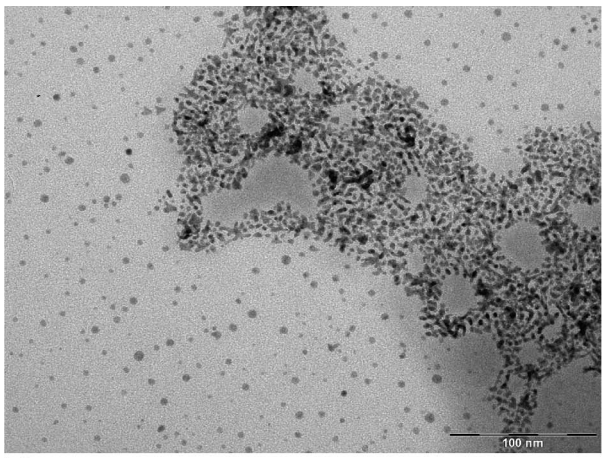

(a)

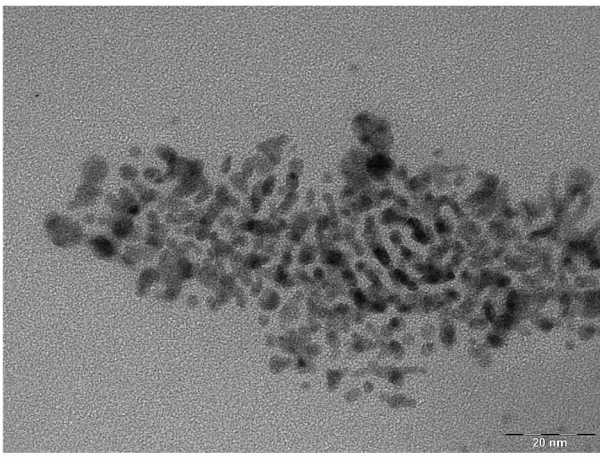

(b)

Fig. 2 TEM micrographs of Rh(0)@HEA16F in water. a) The worm-like structure and isolated NPs. b) Magnification of an area of a).

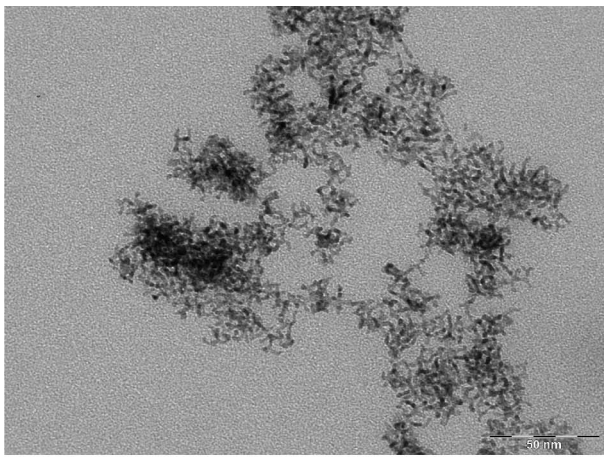

(a)

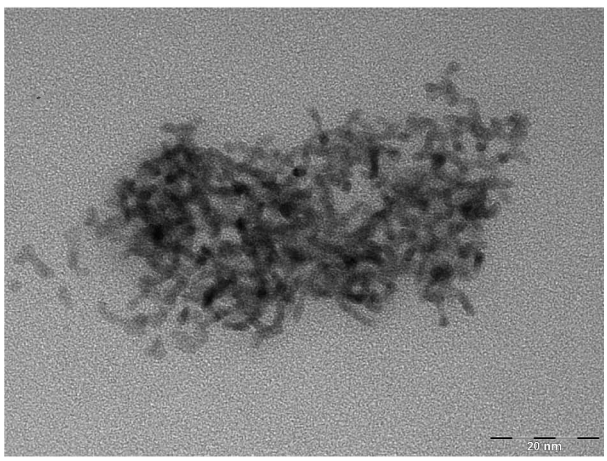

(b)

Fig. 3 TEM micrographs of Rh(0)@HEA16CF_3SO_3 in water. a) Elongated particles (dendrites). b) Magnification of an area showing the elongated forms of the particles.

dendrite morphology has also been proposed in organic media by Chaudret and Philippot.[52–53] Finally, the Rh@HEA16X systems (X = F, BF_4 and CF_3SO_3), organized in extended worm-like NPs or dendrites in aqueous media, have an estimated size of 2–6 nm with a mean diameter of about 3 nm for the "worms". Contrary to these observations, the Rh@HEA16HCO_3 histogram (Fig. 5) resulting from the measurement of about 200 particles shows well-dispersed particles on the grid, with an average diameter of 3 nm, with 75% of the nano-objects included in the range 2.5–3.5 nm. By analogy to carboxylate anion or polycarboxylates, such as citrate polyanions, the hydrogen carbonate derivative HEA16HCO_3 provides a strong and efficient stabilization at the growing NPs' surface. Similar to spherical Rh@HEA16Cl colloids, TEM observation of Rh@HEA16HCO_3 shows a spherical shape with a narrow polydispersity. Finally, based on strong (Cl^- and HCO_3^-) and weak (F^-, BF_4^-, $CF_3SO_3^-$) protection, these comparative TEM studies show the direct influence of the counter anion of the surfactant on the shape, structure and the average particle size.

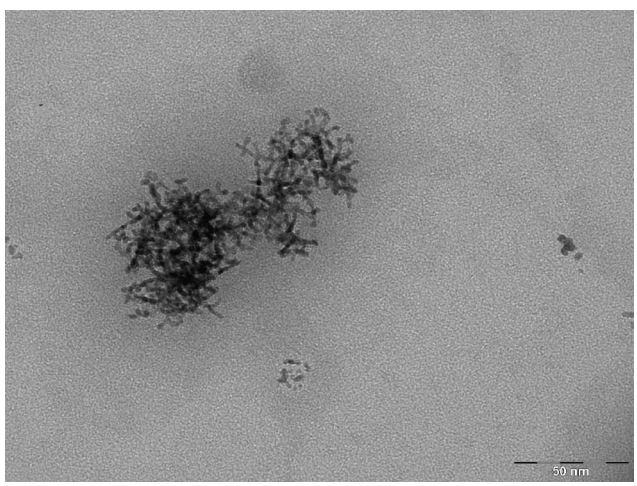

Fig. 4 Worm-like structures obtained with Rh(0)@HEA16BF_4.

The hydrodynamic diameters D_h of the metal colloids coated with various surfactants defined as the Rh(0)@HEA16X systems (Fig. 6) were measured in solution by Dynamic Light Scattering experiments (DLS) and are given in Table 2. The size of the bilayer structure on the particle surface dramatically increased with CF_3SO_3 and BF_4 due to the van der Waals volume of these counter-anions of 80 and 48 $Å^3$, respectively.[54–55] The larger hydrodynamic diameters could also be explained by the extended dendrite shape

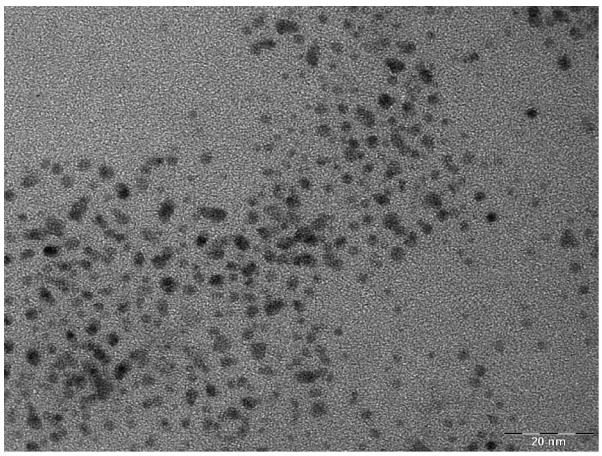

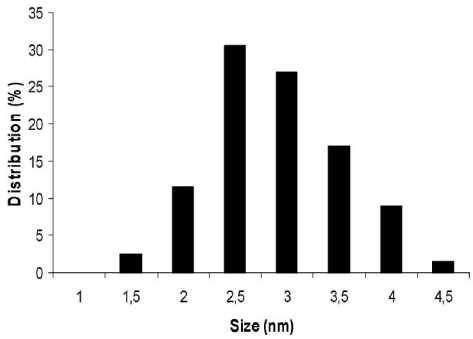

Fig. 5 A TEM micrograph of spherical Rh(0) nanoparticles and a histogram showing the size distribution obtained with $HEA16HCO_3$ as the stabilizer.

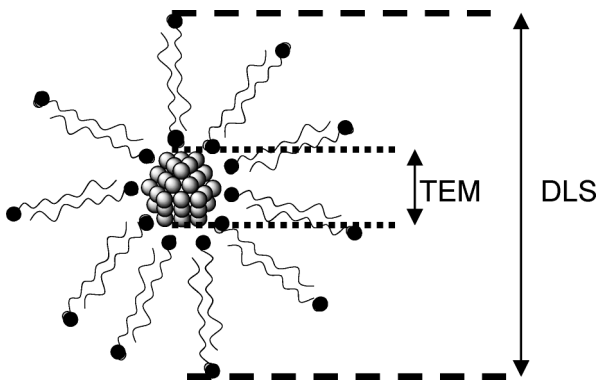

Fig. 6 A schematic representation of the NPs' diameter measured by TEM and the hydrodynamic D_h size using Dynamic Light Scattering.

of the particles (Figs 3 and 4) due to the weaker stabilization during the NPs' growth. In contrast, halogenated surfactants (HEA16Cl and HEA16F) provide a similar hydrodynamic size of around 9 nm. Clearly, a correlation could be established between the structure of the particles (spherical or elongated), the molecular volume of the anion and the D_h value. The smaller spherical nanoparticles obtained with the chloride counter-ion, which provides a strong stabilization, contrast with the elongated colloids obtained with the smaller fluoride anion leading to weakly stabilized species. A higher hydrodynamic diameter D_h is obtained for the hydrogen carbonate anion, which could be correlated to the spherical particles and the growing volume of the anion. Since

Table 2 Number-averaged hydrodynamic diameters D_h and zeta potential ζ data for the surfactant-stabilized Rh nanoparticles

Surfactants	D_h (nm)	ζ (mV)	PDI[a]
HEA16Cl	8.8	+ 40.5	0.14
HEA16F	9.5	+ 43.1	0.20
$HEA16HCO_3$	19.0	+ 50.0	0.29
$HEA16CF_3SO_3$	56.8	+ 42.3	0.22
$HEA16BF_4$	45.4	+ 44.0	0.33

[a] PDI: Polydispersity index PDI < 0.3 monodispersed suspension, PDI > 0.3 polydispersed suspension.

the polydispersity index (PDI) of the hydrodynamic diameter is as low as 0.3, the nanoparticles are produced with a narrow distribution. The zeta potential values of these monodispersed suspensions, which were also measured by electrophoretic light scattering (Table 2), were examined to determine the apparent charge of a nanoparticle in solution. In fact, the surfactants and their counter-ions form an electrical double layer around the rhodium particles and the subshell (stern layer) characterizes the ionic species adsorbed on the particle surface. In all cases, colloids coated with surfactants give a positive charge in solution in the range 40–50 mV.

The obtained surfactant-capped zero-valent Rh nanoparticle dispersions were evaluated in catalytic hydrogenation reactions of various arenes in pure biphasic liquid–liquid (water/substrate) conditions. Alkylated, functionalized and disubstituted derivatives were arbitrarily chosen as model substrates and the hydrogen pressure was established at 20 bar. The Turnover Frequencies (TOFs) were calculated considering an optimized reaction time for the complete conversion of the substrate, and based on the amount of metal introduced and not on the exposed metal surface. Indeed, as previously reported by Janiak et *al.*,[56] the catalytic activity does not purely result from the exposed surface metal atoms, since the surface can restructure, atoms can shift positions during heterogeneous processes and partial aggregation could occur during catalysis, modifying the topology and the fraction of surface atoms. Consequently, the TOFs may be underestimated. The results are summarized in Table 3 according to the nature of the protective agent HEA16X. Independently of the nature of the counter-anion , the partnership of Rh(0)@HEA16X acting as micellar nanoreactors was found to be very pertinent for benzene hydrogenation, with significant activities of up to 3600 h^{-1}. These results could be explained by the higher solubility of benzene in water. Indeed, the solubility of hydrocarbons in water (w/v) at 25 °C decreases in the following order: benzene > toluene > xylene, with values of 1800, 540, 170 ppm respectively.[57] The decreasing activities also correlated with a close combination of the steric hindrance and electron-donor behavior of the substituted substrates in the same order of benzene > anisole ≈ toluene > *o*-xylene. Finally, the HCO_3 anion provides better activity compared to the CF_3SO_3 counter-ion, which gives lower TOFs. This observation could be explained by the fact that the smaller spherical particles obtained with HCO_3^- expose different facets of their crystalline structure, including higher energy facets, which are often more catalytically active. The lowest activities were observed with the metal colloids coated with $HEA16CF_3SO_3$ and $HEA16BF_4$, which have an extended dendrite morphology (Figs 3 and 4). In that case, the sintering of small nanoparticles into

Table 3 The hydrogenation of benzene derivatives under biphasic conditions with Rh nanoparticles stabilized with HEA16X (X = HCO_3, F, CF_3SO_3, BF_4 and Cl as reference)[a]

X	Substrate	Products (yields %)[b]	*t* (h)/TOF [h^{-1}][c]
Cl		Cyclohexane (100)	0.16/1800
HCO_3		Cyclohexane (100)	0.12/2571
F	benzene	Cyclohexane (100)	0.16/1800
BF_4		Cyclohexane (100)	0.08/3600
CF_3SO_3		Cyclohexane (100)	0.16/1800
Cl		methylcyclohexane (100)	0.25/1200
HCO_3		methylcyclohexane (100)	0.16/1800
F	toluene	methylcyclohexane (100)	0.16/1800
BF_4		methylcyclohexane (100)	0.16/1800
CF_3SO_3		methylcyclohexane (100)	0.42/720
Cl		methoxycyclohexane (100)	0.16/1800
HCO_3		methoxycyclohexane (100)	0.16/1800
F	anisole	methoxycyclohexane (100)	0.16/1800
BF_4		methoxycyclohexane (100)	0.50/600
CF_3SO_3		methoxycyclohexane (100)	0.16/1800
Cl		1,2-dimethylcyclohexane *cis* (97) *trans* (3)	0.50/600
HCO_3		1,2-dimethylcyclohexane *cis* (100)	0.50/600
F	*o*-xylene	1,2-dimethylcyclohexane *cis* (100)	0.33/900
BF_4		1,2-dimethylcyclohexane *cis* (100)	0.50/600
CF_3SO_3		1,2-dimethylcyclohexane *cis* (100)	0.84/360

[a] Conditions: catalyst (3.8×10^{-5} mol), substrate (3.8×10^{-3} mol), surfactant (7.6×10^{-5} mol),water (10 mL), 20 bar H_2, ambient temperature (20 °C), stirred at 1500 rpm [b] Determined by GC analysis [c] reaction time (h) and turnover frequency (h^{-1}) defined as mol of H_2 per mol of rhodium per h.

elongated worm-like nanocrystals could reduce the density of those high energy facets and thus decrease the catalytic activity. The selectivity was also evaluated in the reduction of *o*-xylene. The *cis* diastereomer is the major product (97%) with the chloride anion, as previously reported. With X = HCO_3, F, CF_3SO_3, BF_4, the reaction under hydrogen pressure became more selective, with 100% *cis*-compound produced. Undoubtedly, these conditions (20 bar H_2 at room temperature) favour the fast hydrogenation of the substrate and disfavour its desorption during catalysis, thus limiting the production of the *trans*-isomers.[58]

To conclude, the catalytic activity was mostly influenced by a fine and narrow combination of the physico-chemical properties, based on the choice of the counter-ion associated to the ammonium group and their influence on the CMC, hydrodynamic size and zeta potential in opposition to the size and morphologies of the nanoparticles.

The catalytic lifetime of Rh@HEA16Br has previously been reported, showing the pertinent association of surfactant–Rh(0) as a micellar nanoreactor.[35] In the same way, the recyclability of the new Rh(0)@HEA16X systems was checked under atmospheric hydrogen pressure to justify their stability. The influence of the counter-ion on the durability of these nanoreactors in micellar media was studied through successive hydrogenations of two reference substrates, such as toluene and anisole. After a first run, the aqueous phase containing the colloidal suspension was separated from the hydrogenated product by extraction with Et_2O and then reused in a second run. Fig. 7 shows a comparable turnover activity for all of the systems. Consequently, combining $HEA16^+$ salts with X^- ions produces relevant protective agents to maintain rhodium(0) nanoparticles within the aqueous phase during the catalytic process. No agglomerates were visually observed after the recycling step.

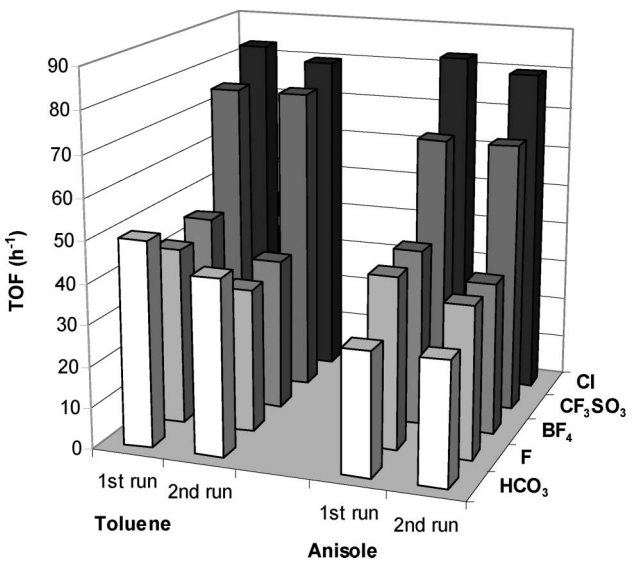

Fig. 7 The activity of the recycled aqueous phase in the hydrogenation of toluene and anisole under 1 bar H_2 and the influence on the nature of the counter-ion.

4. Conclusions

Only a few studies have dealt with the influence of the counter-ions of ionic protective agents for the stabilization of rhodium nanoparticles. Several series have been reported in the protection of iridium colloids in unusual solvents, such as ionic liquids[54,59] or propylene carbonate[29,60] Moreover, common anions, such as Cl^-, BF_4^-, PF_6^-, AcO^-, $citrate^{3-}$ as well as polyoxoanions, were investigated according to the literature. In this paper, we have described original counter-anions of $HEA16^+$ salts providing new micellar

nanoreactors for arene hydrogenations. In particular, HCO_3^-, F^- and $CF_3SO_3^-$ anions of ammonium salts have rarely been reported. The different systems were characterized by adapted physico-chemical experiments (surface tension, DLS technique, TEM analysis). The results confirm that easily prepared, active and reusable green Rh(0) nanocatalysts protected by *N*-cetyl-*N*-(2-hydroxyethyl) ammonium salts constitute an efficient partnership for the reduction of arenes under mild and micellar conditions. No bulk metal or sedimentation were observed during these experiments. The size and the structure of the nanoparticles seem to depend on the nature of the counter-ion and their capacity to provide a strong or weak stabilization at the growing particles' surface. Worm-like Rh(0) nanospecies were observed with fluorinated ions such as F^-, BF_4^- and $CF_3SO_3^-$, whereas isolated and spherical colloids were obtained with Cl^- and HCO_3^- anions leading to relevant activities up to 3600 h^{-1}.

To conclude, we have reported the most important series of counter-ions of hydroxyethylammonium salts described in the literature, and have shown that these new surfactants are efficient capping and stabilizing agents of catalytically active rhodium nanoparticles.

Acknowledgements

This work and Ph. D. grant were supported by the Agence Nationale de la Recherche (ANR), project MesAsColl/ANR-08-CP2D. Thanks to Patricia Beaunier from UPMC for TEM experiments.

Notes and references

1 B. Cornils, *Org. Process Res. Dev.*, 1998, **2**, 121–127.
2 N. Yan, C. X. Xiao and Y. Kou, *Coord. Chem. Rev.*, 2010, **254**, 1179–1218.
3 H. Arzoumanian and D. Nuel, *C. R. Acad. Sci. Paris Ser. II-C*, 1999, **2**, 289–293.
4 A. Denicourt-Nowicki and A. Roucoux, *Curr. Org. Chem.*, 2010, **14**, 1266–1283.
5 A. Nowicki, Y. Zhang, B. Leger, J. P. Rolland, H. Bricout, E. Monflier and A. Roucoux, *Chem. Commun.*, 2006, 296–298.
6 A. Denicourt-Nowicki, A. Ponchel, E. Monflier and A. Roucoux, *Dalton Trans.*, 2007, 5714–5719.
7 C. Hubert, A. Denicourt-Nowicki, A. Roucoux, D. Landy, B. Leger, G. Crowyn and E. Monflier, *Chem. Commun.*, 2009, 1228–1230.
8 J. D. Senra, L. F. B. Malta, A. L. F. Souza, L. C. S. Aguiar and O. A. C. Antunes, *Adv. Synth. Catal.*, 2008, **350**, 2551–2558.
9 S. C. Mhadgut, K. Palaniappan, M. Thimmaiah, S. A. Hackney, B. Torok and J. Liu, *Chem. Commun.*, 2005, 3207–3209.
10 T. Huang, F. Meng and L. M. Qi, *J. Phys. Chem. C*, 2009, **113**, 13636–13642.
11 C. H. Xue, K. Palaniappan, G. Arumugam, S. A. Hackney, J. Liu and H. Y. Liu, *Catal. Lett.*, 2007, **116**, 94–100.
12 Y. Li, E. Boone and M. A. El-Sayed, *Langmuir*, 2002, **18**, 4921–4925.
13 Y. Li and M. A. El-Sayed, *J. Phys. Chem. B*, 2001, **105**, 8938–8943.
14 C. E. Hoppe, M. Lazzari, I. Pardinas-Blanco and M. A. Lopez-Quintela, *Langmuir*, 2006, **22**, 7027–7034.
15 I. Washio, Y. Xiong, Y. Yin and Y. Xia, *Adv. Mater.*, 2006, **18**, 1745–1749.
16 J. Glöckler, S. Klützke, W. Meyer-Zaika, A. Reller, F. J. García-García, H.-H. Strehblow, P. Keller, E. Rentschler and W. Kläui, *Angew. Chem., Int. Ed.*, 2007, **46**, 1164–1167.
17 P. J. Debouttiere, V. Martinez, K. Philippot and B. Chaudret, *Dalton Trans.*, 2009, 10172–10174.
18 T. Akiyama, C. Ibata and H. Fujihara, *Heterocycles*, 2010, **80**, 925–931.
19 F. Gonzaga, S. Singh and M. A. Brook, *Small*, 2008, **4**, 1390–1398.
20 F. Gonzaga, R. D'Souza and M. A. Brook, *Soft Matter*, 2011, **7**, 722–729.
21 H. Bönnemann, K. S. Nagabhushana and R. M. Richards, in *Nanoparticles and Catalysis*, ed. D. Astruc, 2008, pp. 49–91.
22 A. Roucoux, J. Schulz and H. Patin, *Chem. Rev.*, 2002, **102**, 3757–3778.
23 A. Gual, C. Godard, S. Castillon and C. Claver, *Dalton Trans.*, 2010, **39**, 11499–11512.
24 E. J. W. Verwey and J. T. G. Overbeek , *Theory of the Stability of Lyophobic Colloids (second ed.)*, Dover Publications: Mineola, *New York* 1999.
25 A. Roucoux and K. Philippot, in *The Handbook of Homogeneous Hydrogenation*, eds. J. G. de Vries and C. J. Elsevier, 2008, ch. 9, pp. 217–256.
26 S.-H. Wu and D.-H. Chen, *J. Colloid Interface Sci.*, 2004, **273**, 165–169.
27 S. H. Wu and D. H. Chen, *Chem. Lett.*, 2004, **33**, 406–407.
28 B. Nikoobakht and M. A. El-Sayed, *Langmuir*, 2001, **17**, 6368–6374.
29 S. Ozkar and R. G. Finke, *J. Am. Chem. Soc.*, 2002, **124**, 5796–5810.
30 Z. Deng and D. E. Irish, *J. Phys. Chem.*, 1994, **98**, 11169–11177.
31 D. Astruc, F. Lu and J. R. Aranzaes, *Angew. Chem., Int. Ed.*, 2005, **44**, 7852–7872.
32 L. D. Pachón and G. Rothenberg, *Appl. Organomet. Chem.*, 2008, **22**, 288–299.
33 A. Roucoux, A. Nowicki and K. Philippot, in *Nanoparticles and Catalysis*, ed. D. Astruc, 2008, ch. 11, pp. 349–388.
34 J. Schulz, A. Roucoux and H. Patin, *Chem. Commun.*, 1999, 535–536.
35 J. Schulz, A. Roucoux and H. Patin, *Chem.–Eur. J.*, 2000, **6**, 618–624.
36 V. Mevellec, A. Roucoux, E. Ramirez, K. Philippot and B. Chaudret, *Adv. Synth. Catal.*, 2004, **346**, 72–76.
37 C. Hubert, A. Denicourt-Nowicki, J. P. Guegan and A. Roucoux, *Dalton Trans.*, 2009, 7356–7358.
38 A. Nowicki, V. Le Boulaire and A. Roucoux, *Adv. Synth. Catal.*, 2007, **349**, 2326–2330.
39 A. Roucoux, J. Schulz and H. Patin, *Adv. Synth. Catal.*, 2003, **345**, 222–229.
40 S. Dermeik and Y. Sasson, *J. Org. Chem.*, 1989, **54**, 4827–4829.
41 G. Cerichelli, L. Luchetti, G. Mancini and G. Savelli, *Tetrahedron*, 1995, **51**, 10281–10288.
42 B. Léger, A. Nowicki, A. Roucoux and J.-P. Rolland, *J. Mol. Catal. A: Chem.*, 2007, **266**, 221–225.
43 A. Denicourt-Nowicki, M.-L. Romagné and A. Roucoux, *Catal. Commun.*, 2008, **10**, 68–70.
44 Y. Asai, *Chem. Phys. Lipids*, 2003, **124**, 103–109.
45 G. Garofalakis, B. S. Murray and D. B. Sarney, *J. Colloid Interface Sci.*, 2000, **229**, 391–398.
46 R. Nagarajan, *Langmuir*, 2001, **18**, 31–38.
47 B. Winter, R. Weber, I. V. Hertel, M. Faubel, L. Vrbka and P. Jungwirth, *Chem. Phys. Lett.*, 2005, **410**, 222–227.
48 J. N. M. Israelachvilli, D. John Ninham and W. Barry, *J. Chem. Soc., Faraday Trans. 2*, 1976, **72**, 1525–1568.
49 Y. Song, R. M. Garcia, R. M. Dorin, H. Wang, Y. Qiu, E. N. Coker, W. A. Steen, J. E. Miller and J. A. Shelnutt, *Nano Lett.*, 2007, **7**, 3650–3655.
50 L. S. Ott and R. G. Finke, *Inorg. Chem.*, 2006, **45**, 8382–8393.
51 J. D. Aiken, Y. Lin and R. G. Finke, *J. Mol. Catal. A: Chem.*, 1996, **114**, 29–51.
52 E. Ramirez, L. Eradès, K. Philippot, P. Lecante and B. Chaudret, *Adv. Funct. Mater.*, 2007, **17**, 2219–2228.
53 C. Pan, K. Pelzer, K. Philippot, B. Chaudret, F. Dassenoy, P. Lecante and M. J. Casanove, *J. Am. Chem. Soc.*, 2001, **123**, 7584–7593.
54 G. S. Fonseca, G. Machado, S. R. Teixeira, G. H. Fecher, J. Morais, M. C. M. Alves and J. Dupont, *J. Colloid Interface Sci.*, 2006, **301**, 193–204.
55 A. B. McEwen, H. L. Ngo, K. LeCompte and J. L. Goldman, *J. Electrochem. Soc.*, 1999, **146**, 1687–1695.
56 E. Redel, J. Krämer, R. Thomann and C. Janiak, *J. Organomet. Chem.*, 2009, **694**, 1069–1075.
57 M. Matsumoto, Y. Inomoto and K. Kondo, *J. Membr. Sci.*, 2005, **246**, 77–81.
58 S. Siegel and B. Dmuchovsky, *J. Am. Chem. Soc.*, 1962, **84**, 3132–3136.
59 G. Machado, J. D. Scholten, T. d. Vargas, S. R. Teixeira, L. Ronchi and J. Dupont, *Int. J. Nanotechnol.*, 2007, **4**, 541–563.
60 S. Özkar and R. G. Finke, *Langmuir*, 2002, **18**, 7653–7662.